Numerical/Experimental Validation of Thin-Walled Composite Box Beam Optimal Design

(Article begins on next page)

25 April 2024

Numerical/Experimental Validation of Thin-Walled Composite Box Beam Optimal Design

Enrico Cestino [1,*,†] , **Giacomo Frulla** [1,†] , **Paolo Piana** [2,†] **and Renzo Duella** [2,†]

1   Department of Mechanical and Aerospace Engineering, Politecnico di Torino, 10129 Torino, Italy; giacomo.frulla@polito.it
2   Tesco Go SRL, Via Dell'industria 11, 10023 Chieri (TO), Italy; Paolo.Piana@tescogo.it (P.P.); Renzo.Duella@tescogo.it (R.D.)
*   Correspondence: enrico.cestino@polito.it
†   These authors contributed equally to this work.

Abstract: Thin-walled composite box beam structural configuration is representative of a specific high aspect ratio wing structure. The optimal design procedure and lay-up definition including appropriate coupling necessary for aerospace applications has been identified by means of "ad hoc" analytical formulation and by application of commercial code. The overall equivalent bending, torsional and coupled stiffness are derived and the accuracy of the simplified beam model is demonstrated by the application of Altair Optistruct. A simple case of a coupled cantilevered beam with load at one end is introduced to demonstrate that stiffness and torsion angle distribution does not always correspond to the trends that one would intuitively expect. The maximum of torsional stiffness is not obtained with fibers arranged at 45° and, at the maximum torsional stiffness, there is no minimum rotation angle. This observation becomes essential in any design process of composite structures where the constraints impose structural couplings. Furthermore, the presented theory is also extended to cases in which it is necessary to include composite/stiffened hybrid configurations. Good agreement has been found between the theoretical simplified beam model and numerical analysis. Finally, the selected composite configuration was compared to an experimental test case. The numerical and experimental validation is presented and discussed. A good correlation was found confirming the validity of the overall optimization for the optimal lay-up selection and structural configuration.

Keywords: box-beam equivalent model; optimal layup selection; composite optimization

1. Introduction

The introduction of future configurations of unconventional aircraft demand for innovative structural concepts to improve the structural performance, and thus reduce the structural weight. New materials and specific couplings are necessary to cope with such demanding structural design influencing static and dynamic aircraft performances. Moreover, in the design phase, the structural model could be improved by FE (finite element) analysis and numerical optimizations. In particular, the conventional design process can be improved and simplified when a preliminary step in numerical optimization is adopted. The design space for the aeroelastic tailoring is being significantly enlarged with the introduction of innovative solutions such as Variable Angle Tow (VAT) laminates and curvilinear stiffeners [1–5]. Previously experimental/numerical comparisons as in ref [6,7] were discussed pointing out specific post-critical behavior of thin-walled composite wing box under bending and torsion loads. A specific analytical procedure for determining equivalent stiffness of box-beam typical configuration has been developed recently. Innovative configurations accounting for local coupling effects due to the presence of straight and curved stringers have been introduced in [8–11].

Particularly, the local stiffening effects introduced by innovative configurations may allow unconventional structural coupling and postpone critical aeroelastic phenomena otherwise typical of a wing with a High Aspect Ratio (HAR) [2,3,12–14]. An appropriate structural model capable of taking into consideration specific structural behavior of such kind of configurations should be adopted, in order to correctly introduce the terms of geometric nonlinearity in the curvatures of the beam, the effects due to the introduction of the composite material and the effects of local stiffness [12,15–19]. Outcomes obtained within the preliminary stages, where low fidelity models are adopted to navigate the entire design space via optimization or parametric analysis, can be further investigated in the successive design phases, by means of detailed FE analysis.

A three steps strategy is implemented in Altair OptiStruct to optimize composite structures. The main features of the optimization strategy are briefly summarized herein (Figure 1) [20–24]. Phase I, namely Free Size Optimization, is useful during the conceptual design stages. It seeks optimal plies thicknesses and orientations starting with an initial guess which commonly is a quasi-isotropic laminate made by thick plies. The latter are defined as "super plies" within Altair's suite. Phase II begins with the standardization of the thicknesses and orientations considering manufacturing and commercial constraints. It is worth noting that Phase II no longer is a conceptual design stage because it works on component defined geometries and thicknesses. For this stage, the optimization is performed with the Altair's Free Size Optimization method with the Gauge technique. Finally, phase III performs the stacking sequence optimization, i.e., solves the combinatorial optimization problem aiming at attaining the desired performance by shuffling the plies through the laminate thickness. This task is performed using Altair's Shuffle Optimization.
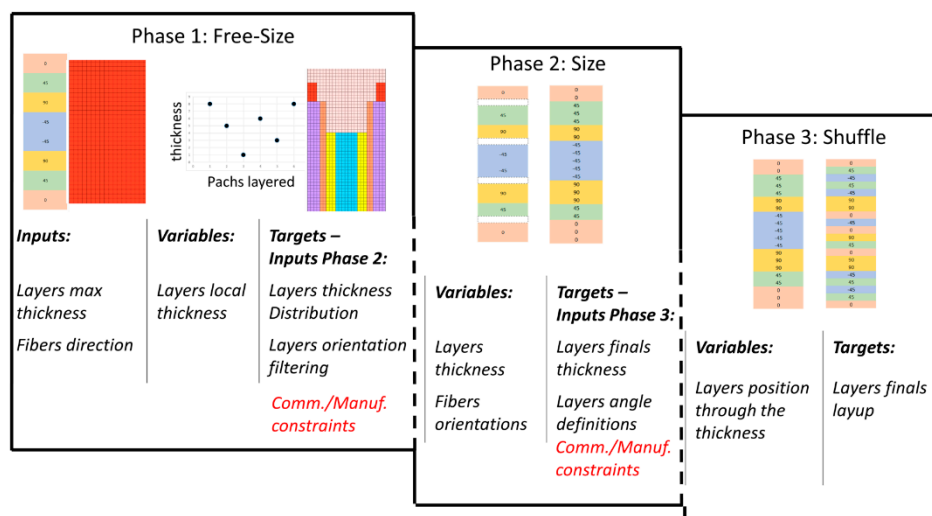

Figure 1. Composite laminate optimization process [22].

The present paper aims to validate the outcomes of a low fidelity beam-wise model previously developed [8–11] and analyze design aspects not clearly highlighted by the available literature in the presence of structural couplings typical of innovative aeroelastic configurations. The validation is two-fold namely: (a) the results obtained with a simplified box-beam model are validated through Altair OptiStruct and, (b) an experiment is carried out to fully assess the outcomes of the low-fidelity model. The final objective of the manuscript is to emphasize the need for an accurate low-fidelity model with respect to cumbersome FE optimization for navigating the design domain during preliminary design stages.

The equivalent beam properties of a single-cell box beam are computed as in [8]. The optimal configuration is identified through a parametric analysis. Concurrently, the optimization is performed using a commercial FE code, namely Altair OptiStruct. Finally, the optimized box-beam is built and tested to assess the numerical results.

2. Equivalent Structural Model for Composite Box-Beams and Numerical Optimization Procedure Description

The beam behavior is described through the longitudinal displacement $u\,(x,\,t)$, the transverse displacement $v\,(x,\,t)$ and $w\,(x,\,t)$, along the y and z axes, respectively, and the torsional angle $\theta\,(x,\,t)$, as shown in Figure 2. Two mutually interrelated coordinate systems are introduced: the first one is the orthogonal Cartesian global coordinate system $(x,\,y,\,z)$ and the second one is the local plate coordinate $(x,\,s,\,n)$ where the n-axis is normal to the middle surface of a plate element, while the s-axis is tangent to the middle surface and is directed along the contour line of the cross-section (Figure 2). A relation between the two coordinate systems can be established as follows (see Appendix A for all the symbols):

$$\vec{r}\,(s,x) = x\,\vec{i}\,_x + y(s)\,\vec{i}\,_y + z(s)\,\vec{i}\,_z = x\,\vec{i}\, + r_n\,\vec{e}\,_n + r_t\,\vec{e}\,_t \tag{1}$$

$$\vec{e}\,_t = \frac{dy}{ds}\vec{i}\,_y + \frac{dz}{ds}\vec{i}\,_z \quad , \quad \vec{e}\,_n = \frac{dz}{ds}\vec{i}\,_y - \frac{dy}{ds}\vec{i}\,_z \quad , \quad r_t = y\frac{dy}{ds} + z\frac{dz}{ds} \quad , \quad r_n = y\frac{dz}{ds} - z\frac{dy}{ds}. \tag{2}$$
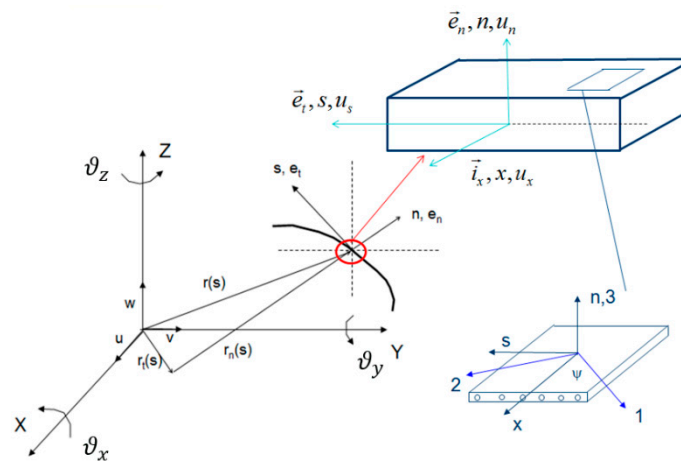

Figure 2. Reference system and sign convention.

In the case of a single-cell, closed cross-section, a homogenization method as in [8–10,12] has been used in calculating the effective properties of reinforced shells and plates. A reduced stiffness matrix has been obtained for a single lamina, starting from the unidirectional/orthotropic composite layer relations in the material system (1,2,3) and applying a simple rotational transformation from the material coordinate system to the *x-s-n* coordinate system [8].

The following assumptions have been introduced: the cross-sections do not deform in their own planes; transverse shear effects are discarded (t/2 h ≤ 0.1, t/2 w ≤ 0.1, 2 w/L ≤ 0.1, 2 h/L ≤ 0.1); a free warping assumption (bi-moment effect discarded), valid for a high aspect ratio wing, has been considered while hoop stress resultants are discarded; the shear flow is considered constant (*Nxs* = cost) in the spirit of the Batho–Bredt theory; the strains are small and the linear elasticity theory has been applied.

Although the membrane approximation is valid in the above range, it would be interesting to investigate the limit of such an approximation and to see whether a modification of the stiffness relations is necessary in certain cases. The mid-plane displacement components u_m, v_m, and w_m of an arbitrary point in the global coordinate system can be expressed as:

$$u_m = u_0 - y(s)\vartheta_z + z(s)\vartheta_y - g(s) \quad , \quad v_m = v_0 - z\vartheta_x \quad , \quad w_m = w_0 + y\vartheta_x \tag{3}$$

where g is a warping correction function and can be determined from the condition that should be a single-valued continuous function as in [12,15]. The local plate stiffness ([A], [B] and [D]) is

determined on the basis of the lamination angle and the stacking sequence. If symmetric lamination holds, $[B] = 0$ and if the circumferential resultant stress and moment are assumed to be zero, according to the thin-walled tube hypothesis, the expressions of the $[A^*]$ and $[D^*]$ matrices are reduced to:

$$
A^*_{11} = A_{11} - \frac{A^2_{12}}{A_{22}}; \quad A^*_{16} = A_{16} - \frac{A_{12}A_{26}}{A_{22}}; \quad A^*_{66} = A_{66} - \frac{A^2_{26}}{A_{22}}
$$
$$
D^*_{11} = D_{11} - \frac{D^2_{12}}{D_{22}}; \quad D^*_{16} = D_{16} - \frac{D_{12}D_{26}}{D_{22}}; \quad D^*_{66} = D_{66} - \frac{D^2_{26}}{D_{22}}.
$$

(4)

Resultant section loads and stiffness matrix are reported in Equations (5) and (6):

$$
\begin{aligned}
F_x &= \oint N_{xx}ds \\
M_x &= \oint N_{xs}r_n(s)ds + 2\oint M_{xs}ds \\
M_y &= \oint N_{xx}z(s)ds + \oint M_{xx}(-dy/ds)ds \\
M_z &= -\oint N_{xx}y(s)ds - \oint M_{xx}(dz/ds)ds
\end{aligned}
$$

(5)

$$
\left\{ \begin{array}{c} F_x \\ M_x \\ M_y \\ M_z \end{array} \right\} = [C] \left\{ \begin{array}{c} e \\ \rho_x \\ \rho_y \\ \rho_z \end{array} \right\} = \left[\begin{array}{cccc} C_{00} & C_{01} & C_{02} & C_{03} \\ C_{01} & C_{11} & C_{12} & C_{13} \\ C_{02} & C_{12} & C_{22} & C_{23} \\ C_{03} & C_{13} & C_{23} & C_{33} \end{array} \right] \left\{ \begin{array}{c} e \\ \rho_x \\ \rho_y \\ \rho_z \end{array} \right\}.
$$

(6)

The $[C]$ matrix in Equation (6) is representative of the membrane contribution and local plate stiffness effect as in [8]. Specific relations, such as those that represent bending torsion coupled configurations (Circumferentially Asymmetric Stiffness (CAS) models) and stiffness coefficients are computed as in Table 1 where the area enclosed by the midline of the contour section is reported. The formulation reported in Table 1 is correctly developed due to the fact that the thin-walled box beam is real. On the contrary, as reported in [11,25] when the thin-walled beam is equivalent to a stiffened 3D configuration, a specific torsional approximation is required. Starting from the definitions of the beam curvatures:

$$
\left\{ \begin{array}{c} \rho_x \\ \rho_y \\ \rho_z \end{array} \right\} = \frac{1}{C_{22}C_{33}C_{11} - C_{33}C^2_{12}} \left[\begin{array}{ccc} C_{22}C_{33} & -C_{33}C_{12} & 0 \\ -C_{33}C_{12} & C_{33}C_{11} & 0 \\ 0 & 0 & C_{22}C_{11} - C^2_{12} \end{array} \right] \left\{ \begin{array}{c} M_x \\ M_y \\ M_z \end{array} \right\} \begin{array}{l} \rho_x = \vartheta'_x \\ \rho_y = -w'' \\ \rho_z = v'' \end{array}.
$$

(7)

Table 1. $[C]$ Matrix stiffness coefficients for CAS configuration in coupled planar bending-torsion.

Stiffness Coefficient	Expression
C_{11}	$\dfrac{4\Omega^2}{\oint(1/A^*_{66})ds} + 4\oint D^*_{66}ds$
C_{12}	$2\Omega\dfrac{\oint(A^*_{16}/A^*_{66})zds}{\oint(1/A^*_{66})ds} - 2\oint D^*_{16}\left(\dfrac{dy}{ds}\right)ds$
C_{22}	$\oint z^2\left(A^*_{11} - \dfrac{A^{*2}_{16}}{A^*_{66}}\right)ds + \dfrac{\left[\oint(A^*_{16}/A^*_{66})zds\right]^2}{\oint(1/A^*_{66})ds} + \oint D^*_{11}\left(\dfrac{dy}{ds}\right)^2 ds$

It is possible to derive the definition of the system compliance from the point of view of the theoretical beam model:

$$
U = \frac{1}{2}\int_0^L \left(M_x\rho_x + M_y\rho_y + M_z\rho_z\right)dx = \frac{1}{2}\int_0^L \frac{C_{11}}{C_{22}C_{11} - C^2_{12}}\left[F(x-L) + F\delta\right]^2 dx
$$

(8)

The compliance value obtained in this way will then be compared successively with the result obtained through Altair OptiStruct. From the experimental point of view, the stiffness of the beam can

be obtained by applying first a unitary force in the z-direction and then a unit torque. The application of the Principle of Virtual works (PLV) provides deflection and rotations:

$$w_z^F = \frac{C_{11}}{C_{22}C_{11}-C_{12}^2}\frac{FL^3}{3} \quad ; \quad \vartheta_x^F = -\frac{C_{12}}{C_{22}C_{11}-C_{12}^2}\frac{FL^2}{2}$$
$$w_z^M = -\frac{C_{12}}{C_{22}C_{11}-C_{12}^2}\frac{M_xL^2}{2} \quad ; \quad \vartheta_x^M = \frac{C_{22}}{C_{22}C_{11}-C_{12}^2}M_xL. \tag{9}$$

and consequently, the components of the stiffness matrix can be determined as follows:

$$\frac{C_{12}}{C_{11}} = -\frac{2L}{3}\left(\frac{\vartheta_x^F}{w_z^F}\right) \quad ; \quad \frac{C_{12}}{C_{22}} = -\frac{2M_x}{F_zL}\left(\frac{\vartheta_x^F}{\vartheta_x^M}\right) \quad ; \quad C_{22} = \frac{F_zL^3}{3}\frac{1}{w_z^F}\frac{1}{\left[1-\left(\frac{C_{12}}{C_{11}}\right)\left(\frac{C_{12}}{C_{22}}\right)\right]}. \tag{10}$$

Once the experimental measurements of the stiffnesses were known, the experimental compliance with the same formula reported in Equation (8) could be evaluated. In the following, because only one experimental flexural test was performed, comparisons will be reported between the theoretical, experimental and FEM analysis only in terms of average deflection and tip rotation when a single force at the end is applied. The comparison in terms of compliance is instead included in the comparison between theoretical and numerical results.

Regarding the optimization procedure, a commercial code is considered: Altair OptiStruct technics Gauge Optimization. Gauge optimization is an iterative process based on gradient methodology applied with Method of Feasible Directions (MFD) algorithm [23,24]. During the numerical process design variable changes during each iteration are limited to a narrow range within their bounds, this guarantees a stable convergence. The end of the iterative process corresponds to optimal design (feasible design) when the convergence criteria are satisfied for two consecutive iterations. This means that for two consecutive iterations, the change in the objective function is less than the objective tolerance and constraint violations are less than 1% [23,24]. The Gauge numerical optimization can be applied to 2D shell elements exclusively and in particular to the thickness or material orientation property variables. In this work, a 3D/2D mixed FE model of composite box beam is developed using shell elements (PCOMP) and hexa elements as shown in Figure 3. The design zones are the upper and lower panels in composite material; these are connected to the steel webs with mesh nodes mapping technique in order to simulate the excellent adhesion of epoxy glue bond joints. Only a small portion of these is defined as no-design space to exclude from the analysis of the constraints-application area. In either the simplified model and in the FE model, the transversal load is applied with an eccentricity of 40 mm with respect to the beam tip according to the experimental test. Numerical optimization is performed to identify the laminate plies angles in order to obtain the most bending-torsion couple effect. The result is reached by optimizer reducing the beam global stiffness to find the maximum of the objective function (compliance) subjected to the beam tip rotation constrain. A summary of the FE model setup is reported the following:

1.   Composite laminate definition and optimization setting: initial lay-up [04] for both plates
2.   Optimization Objective definition: maximum compliance (Equation (8))
3.   Discrete angle definition from –90° to 90°, 1° each iteration
4.   Optimization constraint: tip rotation higher than 0.845° for enhancing bending–torsion coupling.

Considering that, in the FE model with composite laminate (Figure 4a), the plies orientation angle is evaluated turning around the shell element normal direction with the "right-hand rule". The model presented in this work has the composite plates modeled with shell elements that have opposite normal vectors between upper and lower plate, Figure 4b. This condition in order to have a visual simplified post-processing of plies angles during the iterative process: the same ply in the upper plate and lower to have the same orientation should be a positive angle value in the upper plate and the same but negative in the lower.
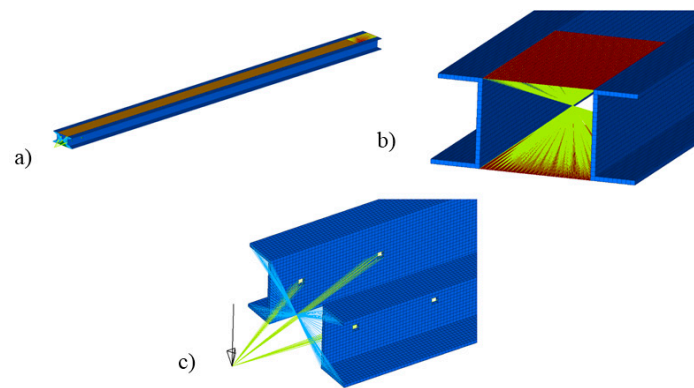
Figure 3. FE model design for the Gauge procedure: (**a**) complete FE model; (**b**) restrain application area; (**c**) load application and beam tip behavior monitoring points.
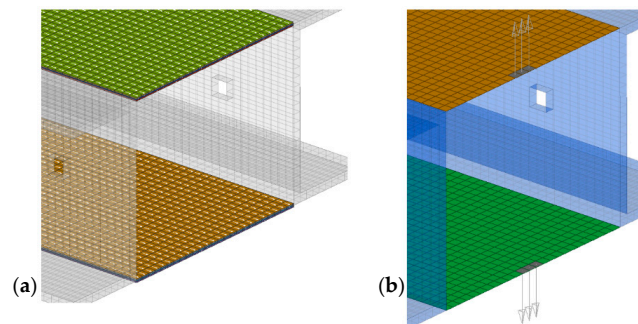

Figure 4. (**a**) Upper and lower plates visualized as a laminate stack; (**b**) normal direction for upper and lower plates shell elements.

3. Test Case Selection and Manufacturing

The sample for testing activity is presented in Figure 5. The Caps of the box-beam are made by T700 Carbon/epoxy prepreg with fibers oriented at 18° (4 layers), 1 mm of the total thickness, corresponding to the optimal value obtained both with the theoretical and numerical model. Cure conditions 2 h at 135 °C. The vertical web is manufactured by standard C-shaped components of aluminum alloy (E = 58,000 MPa v = 0.33). Mechanical properties adopted are: E_1 = 118,000 MPa, E_2 = 9938 MPa; G_{12} = 3400 MPa; v_{12} = 0.31. The upper and lower flanges are manufactured by hand-layup and cured in an autoclave as in Figure 6.
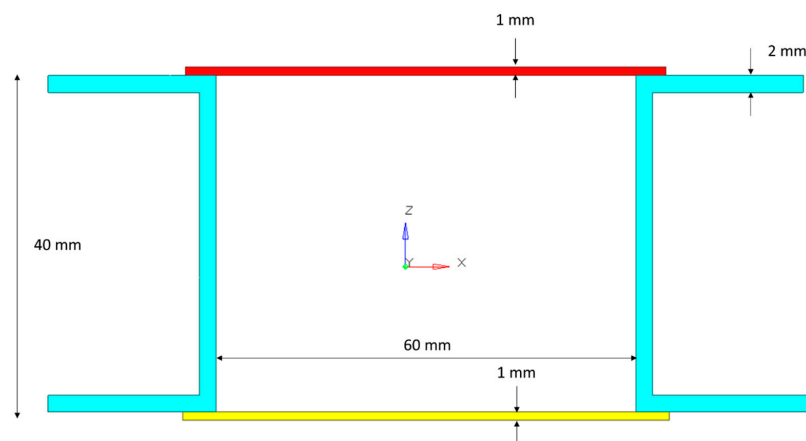

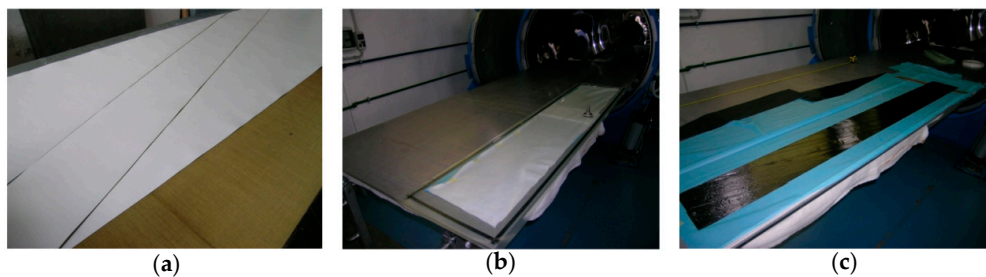**Figure 5.** Typical section of the box-beam for testing.

Figure 6. The technology adopted to manufacture the 18° upper and lower skin: (**a**) single ply cutting (**b**) vacuum bagging preparation (**c**) final carbon/epoxy skin.

The application of the previously described analytical stiffness coefficients provides the determination of the stiffness matrix components as a function of the lamination angle. In the present case, the behavior of the stiffness coefficients is reported in Figure 7. The graph shown in Figure 7a shows a maximum of flexural torsional coupling stiffness ratio (C12/C12max) in correspondence of a CAS type configuration with a ply of the upper and lower faces oriented at about 18°. As expected, however, the configuration with fibers oriented at 0° is the one that maximizes the flexural stiffness ratio (C22/C22max). Always considering a CAS-type configuration, the maximum torsional rigidity ratio (C11/C11max) is obtained with fibers oriented at about 27°. The result was also confirmed by the FEM analysis performed at different ply angles orientation where the beam stiffness is obtained by evaluating rotation and flexural displacement at the tip when only one shear force or twisting moment is applied. The calculation of the stiffness is subsequently obtained through the application of Equation (10). It is also interesting to note from Figure 7b that the maximum rotation angle is obtained with a ply angle of 12° different from 18°, maximum deflection is still obtained with a ply angle of 45°. The 18° angle is the one that satisfies the indicated optimal problem that couples the maximum compliance with the maximum angle of rotation and was selected for the experimental test.
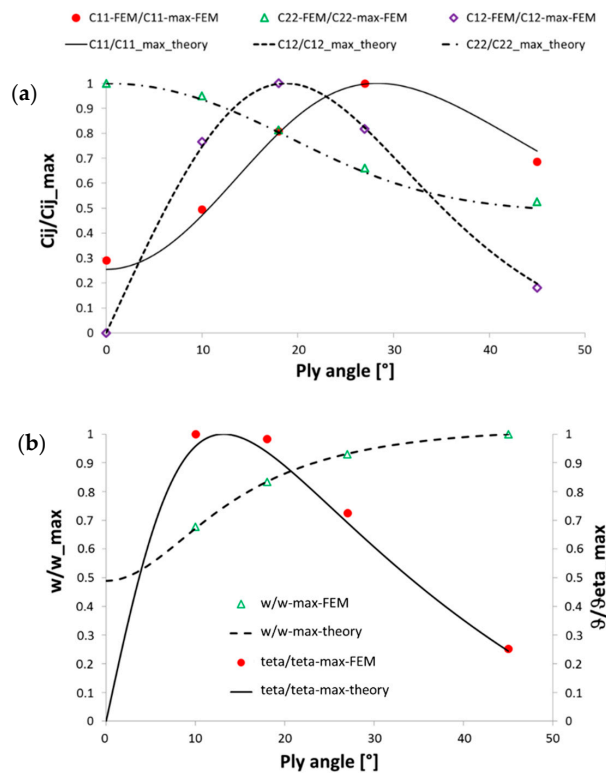

Figure 7. (**a**) Stiffness coefficients for the selected configuration vs. ply angle (**b**) deflection (w) and rotation (ϑ) vs. ply angle.

4. Numerical/Experimental Comparison and Validation

The selected test case has been loaded as a cantilever beam (Figure 8) measuring the tip deflection and torsion. The analytical results, numerical results and the experimental ones are compared in Figure 9. The box-beam has been simulated by the FEM procedure using consistent laminate lay-up.

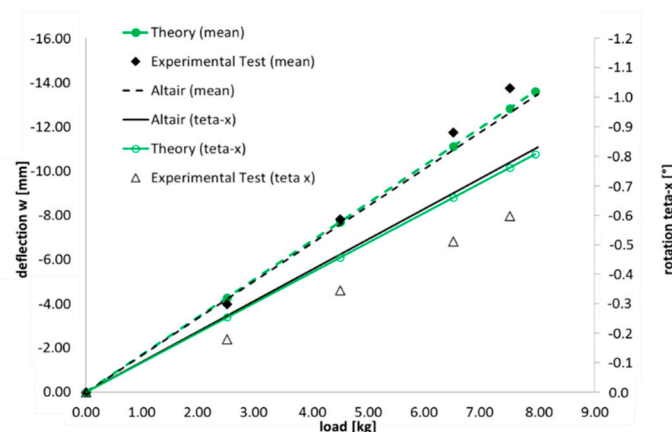

Figure 8. Experimental set-up.

Figure 9. Fem and theoretical results vs. experimental results.

Similar behavior was obtained for both theoretical and experimental results, Figure 9 shows the deflection and rotation of the center of the tip section, obtained from the displacements measured by the two transducers. The main differences can be attributed to the variability of the data related to the considered composite material and to a not perfect correspondence between the clamped constraint and load system in the theoretical and numerical model with respect to the experimental case.

In order to validate the theoretical methodology and to correlate the experimental test results obtained in the Polytechnic laboratory with a numerical simulation, an optimization with Altair Optistruct software has been performed. The boundary conditions are implemented in order to simulate the experimental test load condition with a maximum load equal to 8 kg. Gauge technique allows the optimization of a singular feature of element property such as thickness for PSHELL and each orientation angle/layer thickness for PCOMP 2D elements. In this work, numerical optimization was used in order to check and validate the theoretical results about the layer angle on torsion capabilities. The Gauge technique has been applied to identify the optimal layer angle in order to obtain the maximum bending–torsion couple effect for the box-beam.

The initial condition used is a box beam with upper and lower panels made by unidirectional laminate with fibers oriented at 0°. It is worth noting that this initial configuration yields no bending–torsion coupling.

The Gauge optimization is an iterative process based on gradient methodology, an efficient and consolidated approach to optimize the aerospace composite material components such as described in [26].

Figure 10 reports the comparison between the results obtained by the optimizer and the theoretical reference as a function of iterations. The compliance computation demonstrated that the composite beam model, despite assumptions adopted (transverse shear warping effect discarded, symmetric configuration $[B] = 0$ adopted) presents a comparable energy contribution with the FEM model where all these effects are included, demonstrating the validity of the assumptions.

Comparison is performed on global stiffness matrix coefficients related to flexural stiffness (C22), torsional stiffness (C11) and coupling stiffness (C12). For numerical results, these coefficients are evaluated from $[A]$ and $[D]$ laminate stiffness matrices using formulas reported in Table 1. The stiffness plots report a very good convergence of numerical values to the reference point obtained theoretically with all layers at 18°.

The last iteration shows a tip rotation of about 0.845° and deformation energy (compliance) of about 542.5 J corresponding to 8 kg load.
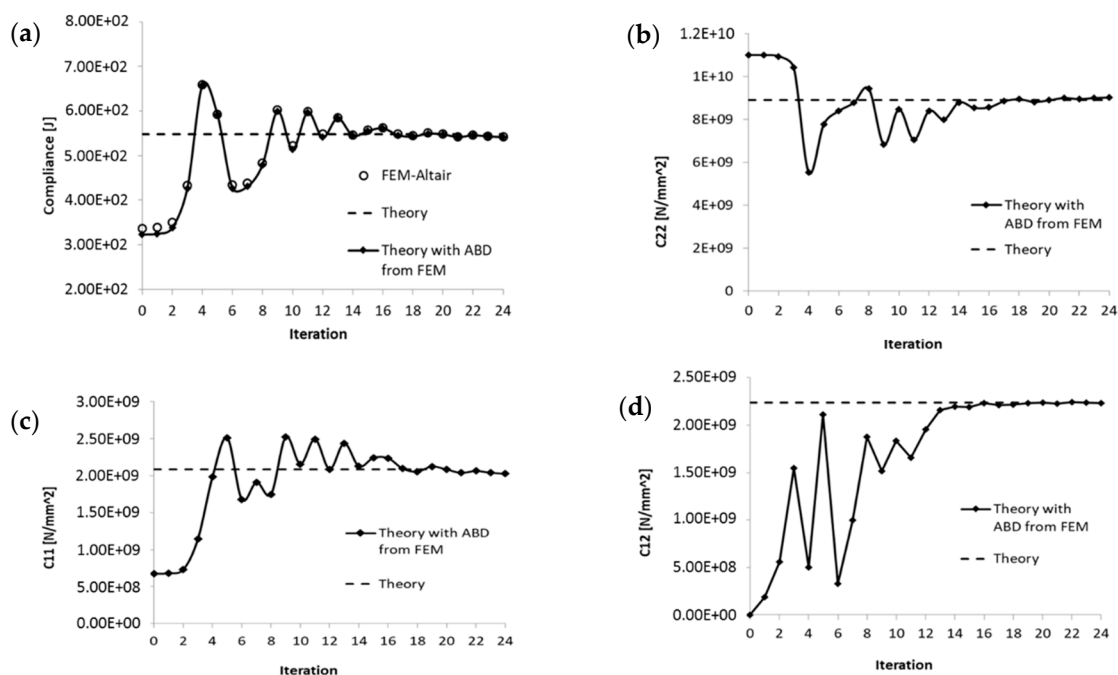

Figure 10. Gauge optimization graphs results: (**a**) Compliace; (**b**) Bending stiffness; (**c**) Torsional stiffness; (**d**) Coupling stiffeness.

FEA results of box beam layered with the optimal layup obtained from numerical optimization show displacement and rotational fringe with linearity counters, with the maximum effect of bending-torsion coupled effect evident on the box beam tip (Figure 11). The optimum condition is asymptotic at the level of global stiffnesses as shown in Figure 10. Low difference in plies orientation between the numerical best results (24th iteration) and the previous lay-ups is allowed as it does not contribute to an appreciable deviation in stiffness. The asymptotic behavior is confirmed also by torsion angle analysis along with the numerical iteration, where the difference through tip rotation at iterations 22 and 24 is less than 1%.

The lamination obtained with the feasible design result at iteration 22 is very close to the theoretical optimum lay-up (all 18°), as reported in Table 2 and Figure 12. The lower plate of box beam optimized numerically has 3 to 4 layers difference to reference layup while the upper plate has all the layers at 17°. All plies have orientation values very close to theoretical reference therefore the theoretical result can be evaluated obtained by a robust methodology. Maximum variation is obtained at layer 4 of the lower plate where an optimum of −16° is obtained respect to the theoretical −18°.

Table 2. Ply angles of best results by theoretical approach, gauge optimization (iterations 22th and 24th).

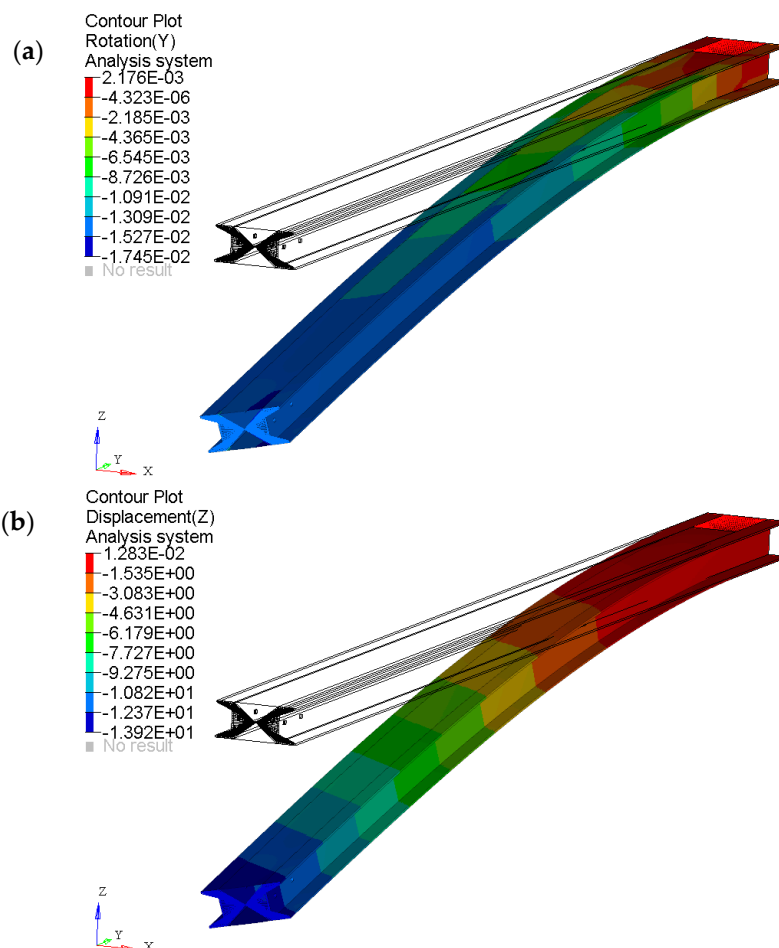| Analytical Optimum		Iteration 22th		Iteration 24th	
Ply	**Angle (°)**	**Ply**	**Angle (°)**	**Ply**	**Angle (°)**
Up_1	18	Up_1	18	Up_1	17
Up_2	18	Up_2	18	Up_2	17
Up_3	18	Up_3	18	Up_3	17
Up_4	18	Up_4	18	Up_4	17
Low_1	−18	Low_1	−17	Low_1	−18
Low_2	−18	Low_2	−17	Low_2	−17
Low_3	−18	Low_3	−18	Low_3	−18
Low_4	−18	Low_4	−16	Low_4	−16
		tip rotation	0.83867°	tip rotation	0.84527°

Figure 11. FE analysis results of box beam numerical optimum lay-up: (**a**) Y-rotation result; (**b**) Z-deflection result.
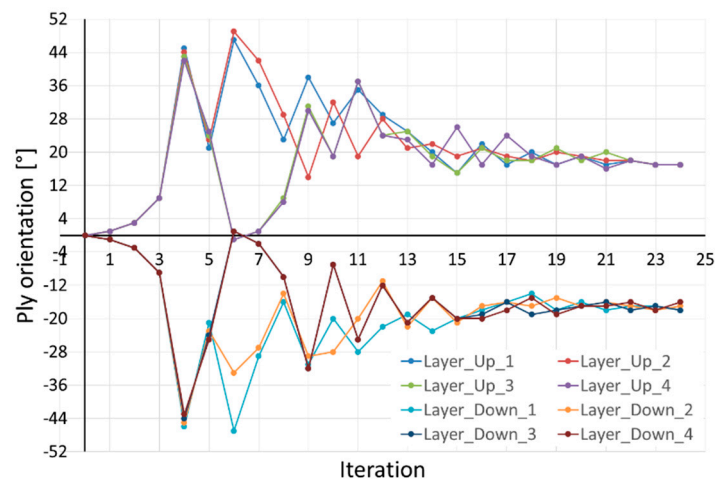
Figure 12. Graph with the angles ply iterative process.

5. Conclusions

The validation of the optimal configuration for a hybrid isotropic/composite box-beam has been presented. The performances offered by the optimal beam configuration obtained with a low-fidelity beam model have been compared against those of a high-fidelity model synthesized using Altair OptiStruct and with an experiment. The selected structural performance expected by the low fidelity model of a composite/aluminum thin-walled box-beam, specifically selected for the validation, is investigated. The numerical optimization and experimental configuration results are compared in order to confirm the validity of the selected procedure. The maximizing of slender box-beam compliance in order to obtain the plies orientation angle correlated to maximum bending/torsion effect is imposed in both methodologies.

A simple case of a coupled cantilevered beam with load at one end is introduced. Maximum of flexural torsional coupling stiffness ratio was obtained with a ply of the upper and lower faces oriented at about 18° while the maximum torsional rigidity ratio was obtained with fibers oriented at about 27° and maximum rotation obtained with a ply angle of 12° different from 18°.

These types of considerations obtained by low fidelity models are fundamental in any design of innovative aeroelastic configurations and not fully investigated by open literature.

The low-fidelity model (simplified beam-model) results are in good agreement with the high-fidelity model (FE model), confirming the validity of initial assumptions. The comparison with the experimental test shows a certain difference presumably due to uncertainties about the mechanical properties of the composite laminate and constraint conditions. However, a similar torsional–bending coupling behavior is clearly shown. In closure, it has been shown that low-fidelity has to be preferred with respect to accurate models within early design stages to identify promising solutions to be further investigated in the successive design stages.

Appendix A. List of symbols

$\vec{r}\ \vec{i}_{x,y,z}$	Position and unit vectors in the x, y, z reference system
$r_n, \vec{e}_n\ ; r_t, \vec{e}_t$	Position and unit vectors in the x, s, n reference system
$\vartheta_{x,y,z}$	Rotations respect to x, y, z axis
u_n, u_s, u_x	Displacements along n, s, x directions
u_m, v_m, w_m	Midplane displacements in the global coordinate system
u_0, v_0, w_0	Beam centroid displacements in the global coordinate system
$A_{ij}\ ;\ D_{ij}$	Plate membrane and bending stiffness
$F_x; M_{x,y,z}$	Resultant beam section loads
C_{ij}	Beam stiffness
$\rho_{x,y,z}$	Beam curvatures
w	Bending deflection
$t, 2h, 2w$	Typical beam section thickness, width and height
g	Warping function
w_z^F	Vertical deflection due to a tip force
w_z^M	Vertical deflection due to a tip torsion moment
ϑ_x^F	Rotation due to a tip force
ϑ_x^M	Rotation due to a tip torsion moment
U	Compliance

References

1. Gürdal, Z.; Tatting, B.F.; Wu, C.K. Variable stiffness composite panels: Effects of stiffness variation on the in-plane and buckling response. *Compos. Part A Appl. Sci. Manuf.* **2008**, *39*, 911–922. [CrossRef]
2. Kapania, R.K.; Li, J.; Kapoor, H. Optimal Design of Unitized Panels with Curvilinear Stiffeners. In Proceedings of the 5th Aviation, Technology, Integration, and Operations Conference (ATIO), Hyatt Regency Crystal City, Arlington, VA, USA, 26–28 September 2005.
3. Benscoter, S.U.; MacNeal, R.H. *Equivalent Plate Theory for a Straight Multicell Wing*; 2786; NACA TN: Hanover, MD, USA, September 1952.
4. Jaunky, N.; Knight, N.F., Jr.; Ambur, D.R. Formulation of an Improved Smeared Stiffener Theory for Buckling Analysis of Grid-Stiffened Composite Panels. *Compos. B. Eng.* **1996**, *27B*, 519–526. [CrossRef]
5. Jutte, C.V.; Stanford, B.K. *Aeroelastic Tailoring of Transport Aircraft Wings: State-Of-The-Art and Potential Enabling Technologies*; 218252; NASA TM: Hanover, MD, USA, 1 April 2014.
6. Romeo, G.; Frulla, G. Nonlinear Analysis of Graphite/Epoxy Wing Boxes under Pure Bending Including Lateral Pressure. *J. Aircr.* **1995**, *32*, 1375–1381. [CrossRef]
7. Romeo, G.; Frulla, G.; Busto, M. Nonlinear Angle of Twist of Advanced Composite Wing Boxes under Pure Torsion. *J. Aircr.* **1994**, *31*, 1297–1302. [CrossRef]
8. Cestino, E.; Frulla, G. Analysis of slender thin-walled anisotropic box-beams including local stiffness and coupling effects. *Aircr. Eng. Aerosp. Technol.* **2014**, *86*, 345–355. [CrossRef]
9. Cestino, E.; Frulla, G.; Duella, R.; Piana, P.; Pennella, F.; Danzi, F. Application of structural topology optimization to couple thin-walled stiffened box-beams. *SAE Tech. Pap.* **2017**. [CrossRef]
10. Danzi, F.; Cestino, E.; Frulla, G.; Gibert, J. Equivalent Plate Model of Curvilinear Stiffened Panels. In Proceedings of the 7th International Conference on Mechanics and Materials in Design, Albufeira, Portugal, 11–15 June 2017.
11. Danzi, F.; Cestino, E.; Frulla, G.; Gibert, J.M. Numerical and experimental validation of unitized beam model. In Proceedings of the 31st International Congress of the Aeronautical Sciences (ICAS), Belo Horizonte, Brazil, 9–14 September 2018.
12. Cestino, E.; Frulla, G. Critical Aeroelastic Behaviour of Slender Composite Wings in an Incompressible Flow. In *Composite Materials in Engineering Structures*; Davis, J.M., Ed.; Nova Science Publishers, Inc.: Hauppauge, NY, USA, 2020.
13. Romeo, G.; Frulla, G.; Cestino, E.; Marzocca, P. Non-linear Aeroelastic Behavior of Highly Flexible HALE Wings. In Proceedings of the 25th International Congress of the Aeronautical Sciences (ICAS), Hamburg, Germany, 3–8 September 2006.

14. Romeo, G.; Danzi, F.; Cestino, E. Multi-objective optimization of the composite wing box of solar powered HALE UAV. In Proceedings of the 29th Congress of the International Council of the Aeronautical Sciences, St. Petersburg, Russia, 7–12 September 2014.

15. Berdichevsky, V.; Armanios, E.A.; Badir, A.M. Theory of Anisotropic Thin-walled Closed-cross-section Beams. *Compos. Eng.* **1992**, *2*, 411–432. [CrossRef]

16. Armanios, E.A.; Badir, A.M. Free vibration analysis of anisotropic thin-walled closed-section beams. *AIAA J.* **1995**, *33*, 1905–1910. [CrossRef]

17. Librescu, L.; Song, O. *Thin-Walled Composite Beams: Theory and Application*; Springer: New York, NY, USA, 2006; ISBN 978-1-4020-4203-4.

18. Reddy, J.N. *Energy and Variational Methods in Applied Mechanics*; Wiley-Interscience: New York, NY, USA, 1984; ISBN 978-0-471-89673-9.

19. Reddy, J.N. *Mechanics of Laminated Composite Plates: Theory and Analysis*; CRC Press: Boca Raton, FL, USA, 1997; ISBN 9780849331015.

20. Zhou, M.; Fluey, R.; Willmet, T. Multiple phase optimization of composite structures. In Proceedings of the 9th US National Congress of Computational Mechanics, San Francisco, CA, USA, 23–26 July 2007.

21. Zhou, M.; Dias, W. Composite design optimization—from concept to ply-book details. In Proceedings of the 8th World Congress of Structural and Multidisciplinary Optimization, Lisbon, Portugal, 1–5 June 2009.

22. Zhou, M.; Fluery, R.; Kemp, M. Optimization of Composite—Recent Advances and Application. In Proceedings of the 13th AIAA/ISSMO Multidisciplinary Analysis Optimization Conference, Fort Worth, TX, USA, 13–15 September 2010. [CrossRef]

23. *Academic Program, Practical Aspects of Structural Optimization, A Study Guide*, 2nd ed.; Altair Engineering: Troy, MI, USA, 2015.

24. Altair HyperWorks, Help Material, Altair. 2016. Available online: https://sso.altair.com/ (accessed on 27 June 2020).

25. Nemeth, M.P. *A Treatise on Equivalent-Plate Stiffnesses for Stiffened Laminated-Composite Plates and Plate-Like Lattices*; 216882; NASA TP: Hanover, MD, USA, 1 January 2011.

26. Dababneh, O.; Kipouros, T.; Whidborne, J.F. Application of an Efficient Gradient-Based Optimization Strategy for Aircraft Wing Structures. *Aerospace* **2018**, *5*, 3. [CrossRef]